RSC Advances

PAPER

View Article Online
View Journal | View Issue

Cite this: *RSC Adv.*, 2019, **9**, 30932

Impact of metallic trace elements on relaxivities of iron-oxide contrast agents

Ji Ma and Kezheng Chen *

Received 9th September 2019
Accepted 23rd September 2019

DOI: 10.1039/c9ra07227f

rsc.li/rsc-advances

In this work, well-defined 3 nm-sized Ca^{2+}, Fe^{3+}, Na^{+}, Mg^{2+}, Zn^{2+}, Ni^{2+}, Co^{2+}, and Cd^{2+} cation-adsorbed Fe_3O_4/γ-Fe_2O_3 nanoparticles were used as prototype systems to investigate the influence of metallic trace elements in body fluids on the relaxivities of iron-oxide contrast agents. It was found that surface-adsorbed cations formed a deterioration layer to induce pronounced relaxivity loss. Theoretical study showed that such relaxivity loss can be well described by a modified GCAS function, taking into account the harmonic cation oscillations around Fe_3O_4/γ-Fe_2O_3 nanoparticles. Quantum mechanics analyses revealed that even-parity and odd-parity states of harmonic oscillations are dominant in r_1 and r_2 relaxivities, respectively. Moreover, the harmonic oscillations of Na^{+} and Mg^{2+} cations around Fe_3O_4/γ-Fe_2O_3 nanoparticles are found to be classical forbidden, which are quite different from their counterparts located in the classical permissive area.

Introduction

During the last decade or so, magnetic resonance imaging (MRI) has become a vital non-invasive technique that aims to obtain high-resolution anatomical images for diagnosing various kinds of diseases.[1–6] In this scenario, contrast agents are widely employed based on the fact that they can enhance the image contrast in designated regions with brighter or darker signals,[7,8] and hence greatly boosting imaging sensitivity in MRI. Despite strenuous and unremitting efforts towards exploring new contrast agents, two tough issues have still been lingering around and plaguing academia. The first one is MRI artifacts, which are always undesirable but unavoidable due to signals yielding from calcification, haemorrhage, blood clot, fat, air, and so forth.[9,10] These artifacts are sometimes indistinguishable from the MRI signals of the applied contrast agents, and probably result in the inaccurate interpretation for the diagnosis. Although various techniques have been developed to suppress artifacts by means of resonant radio frequency tuning,[11,12] successful applications of these techniques are very limited.[13–16] The second pressing issue is mainly related to *in vivo* surroundings, in which the adsorption of macroelements and trace elements onto the contrast agents in body fluids may greatly alter their MRI properties determined from *in vitro* tests. This means that the well-defined MRI performance of as-prepared contrast agents may not be realized or even real in clinical application due to the presence and adsorption of elements in complex fluid environments. This is an important but poorly understood matter open to discussion.

Given that these two tough issues are mainly related to the complicated *in vivo* environments, therefore, in this work, we study the influence of metallic trace elements in fluids on relaxivities of iron-oxide contrast agents. Basically, trace elements in human body can be divided into three types: (i) essential trace elements, including iodine, zinc, selenium, copper, molybdenum, chromium, cobalt, and iron elements; (ii) possibly essential trace elements, including manganese, silicon, boron, vanadium, and nickel elements; (iii) potentially toxic elements but essential in their low dose, including fluorine, lead, cadmium, mercury, arsenic, aluminium, and tin elements. In this study, Fe^{3+}, Zn^{2+}, Co^{2+} (type i), Mg^{2+}, Ni^{2+} (type ii), Cd^{2+} (type iii) cations together with two macroelements (Ca^{2+} and Na^{+} cations) were chosen as typical elements to separately adsorb onto negatively charged 3 nm-sized Fe_3O_4/γ-Fe_2O_3 contrast agents. Relaxivity measurements were then performed to demonstrate relaxivity loss and its variation rule after adsorption of various metallic cations.

Results and discussion

The XRD pattern of the as-synthesized pristine product in Fig. 1(a) shows the presence of Fe_3O_4 (JCPDS no. 85-1436) phase or γ-Fe_2O_3 (JCPDS no. 39-1346) phase, or both. Further, XPS spectrum in Fig. 1(b) gives two distinct peaks at ~711 and ~724 eV corresponding to $Fe2p_{3/2}$ and $Fe2p_{1/2}$ levels, respectively.[17] Two satellite peaks around 718 and 732 eV demonstrate the existence of γ-Fe_2O_3 phase,[18] indicating that the pristine product is a hybrid of both Fe_3O_4 phase and γ-Fe_2O_3 phase. The TEM study shows that pristine Fe_3O_4@γ-Fe_2O_3 particles are

Lab of Functional and Biomedical Nanomaterials, College of Materials Science and Engineering, Qingdao University of Science and Technology, Qingdao 266042, China. E-mail: kchen@qust.edu.cn; Fax: +86-532-84022509; Tel: +86-532-84022509

near spherical [inset of Fig. 1(a)], with an average diameter around 3 nm. These 3 nm-sized Fe_3O_4@γ-Fe_2O_3 particles possess negatively charged surfaces with a zeta potential value of −27.6 mV, which is of benefit to cation adsorption in aqueous solutions. Prior to the impregnation of these bare nanoparticles into various cation stock solutions, control experiments on relaxivities were carried out for these pristine Fe_3O_4/γ-Fe_2O_3 nanoparticles. Fig. 1(c) shows r_1 and r_2 relaxivities are determined (from slopes) to be 3.86 and 17.41 s^{-1} $mmol^{-1}$ L, respectively, with an r_2/r_1 ratio of 4.51. Although these values are barely comparable to Magnevist (a commercial gadolinium complex, $r_1 = 4.6$ s^{-1} $mmol^{-1}$ L, $r_2 = 4.5$ s^{-1} $mmol^{-1}$ L, $r_2/r_1 \sim 1$)[19,20] and much inferior to commercial Feridex ($r_2 = 109.4$ s^{-1} $mmol^{-1}$ L),[1] the optimization of relaxivities and development of new contrast agents are outside the scope of this work.

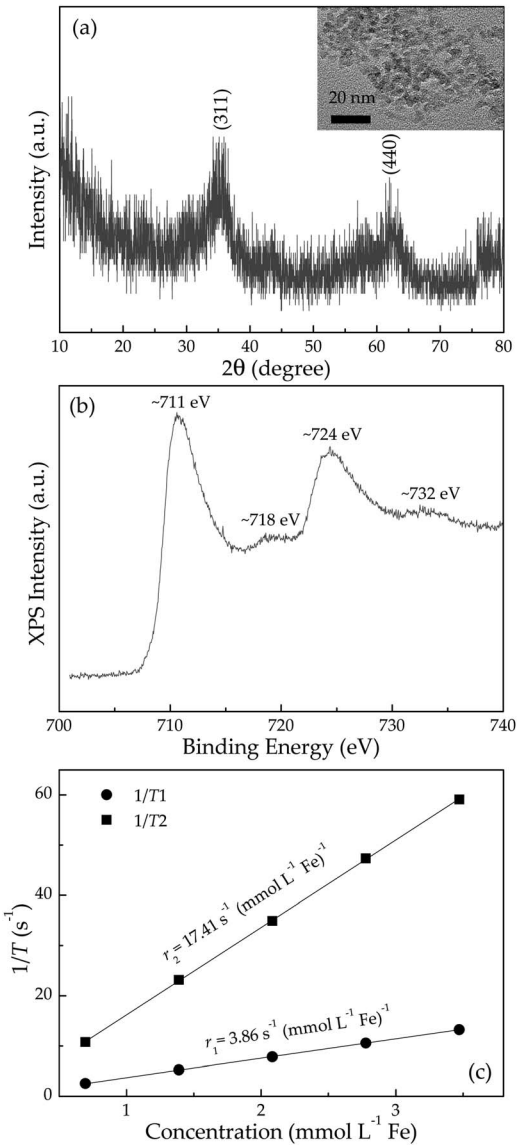

Fig. 1 (a) XRD pattern, TEM image (inset), (b) XPS spectrum and (c) proton longitudinal r_1 and transverse r_2 relaxivities (measured at 1.41 T and 37 °C) of pristine Fe_3O_4/γ-Fe_2O_3 nanoparticles.

After various cation adsorptions, all r_1 relaxivities and most r_2 relaxivities drastically fall into decline (Fig. 2), indicating the degradation of MRI performance of Fe_3O_4/γ-Fe_2O_3 nanoparticles. That is to say, the inevitable adsorption of ions in body fluids in clinical application may well deteriorate the as-designed MRI properties from *in vitro* tests. In this scenario, the quantitative research on the variation of r_1 and r_2 relaxivities after adsorption of various metallic cations is of fundamental importance to predicting MRI performance for *in vivo* applications.

Based on observations in Fig. 2, the surface-adsorbed metallic cations form a deterioration layer on relaxivities of Fe_3O_4/γ-Fe_2O_3 nanoparticles. Therefore, simplifications like independency between adsorbed cationic shell and interior iron-oxide core will not yield the accurate results and are full of fallacies. Along this line, it is essential to consider synergetic interactions between adsorbed cations and particle surfaces from a microscopic standpoint, and even to consider stochastic dependence between electrons and ions at a more microcosmic level. We can describe this idea more precisely in the following way: consider an electrostatically adsorbed cation vibrating at an iron-oxide particle

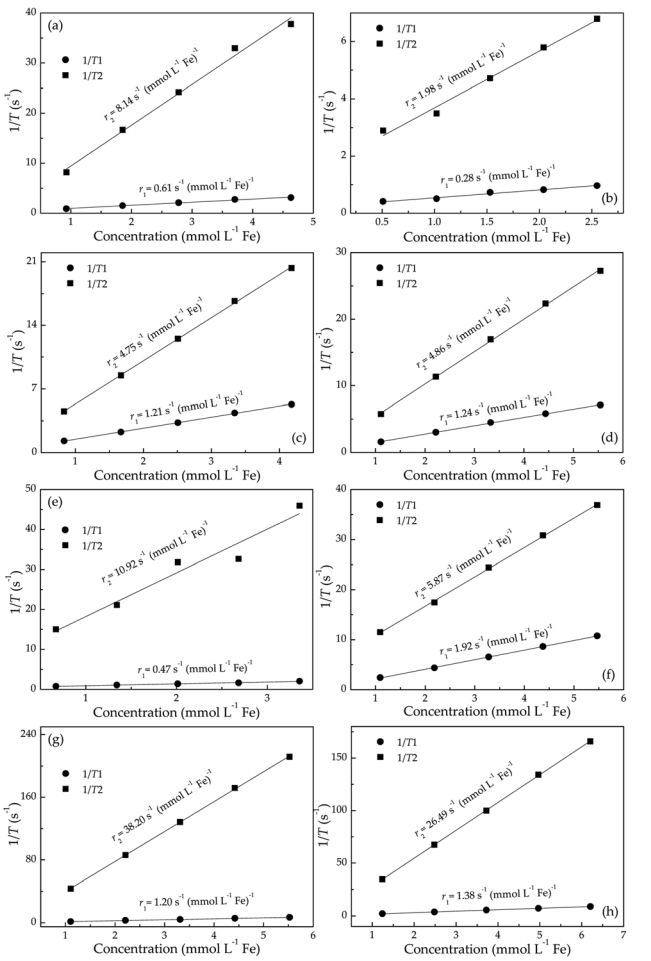

Fig. 2 Proton longitudinal r_1 and transverse r_2 relaxivities (measured at 1.41 T and 37 °C) of (a) Ca^{2+}, (b) Fe^{3+}, (c) Na^{+}, (d) Mg^{2+}, (e) Zn^{2+}, (f) Ni^{2+}, (g) Co^{2+}, and (h) Cd^{2+} adsorbed Fe_3O_4/γ-Fe_2O_3 nanoparticles.

surface. It becomes common sense that any three-dimensional vibration can always be decomposed into numerous one-dimensional harmonic vibrations. In this sense, we draw lessons from conclusions in quantum mechanics and use Hermite polynomials, which belong to a classical orthogonal polynomial sequence, to make the association between final relaxivities and a defined parameter Xr/Z of adsorbed cations. Here, X, r and Z denote electronegativity, radius and atomic number of the cation under discussed (Table 1), respectively. The constructed function of Xr/Z-dependent relaxivity distribution is based on the probability density function utilized in Gram–Charlier A series (GCAS) with some modifications. As known, GCAS function can also be expressed by using Hermite polynomials but it is not guaranteed to be positive, and is therefore not a valid probability distribution. It does not converge in many cases of interest, making it not a true asymptotic expansion, because it is not possible to estimate the error of the expansion. Based on the preceding analyses, the relaxivities r_k ($k = 1$ or 2) can be given by

$$r_k = r_{k0} + \frac{A}{w\sqrt{2\pi}}\, e^{-z^2/2}\left(1 + \left|\sum_{i=0}^{4}\frac{a_i}{i!}H_i(z)\right|\right) \quad (1)$$

wherein z has an expression of $(x - x_c)/w$ ($x = Xr/Z$), a_i are cumulants and A, w are constants. The low-order Hermite polynomials involved in eqn (1) are $H_0 = 1$, $H_1 = 2z$, $H_2 = 4z^2 - 2$, $H_3 = z^3 - 3z$, and $H_4 = z^4 - 6z^3 + 3$.

By applying eqn (1), the experimental data of both r_1 and r_2 relaxivities for various adsorbed cations can be separately connected with smooth curves, as shown in Fig. 3(a) and (b), respectively. The correlation coefficient R^2 values of the fitting plots are beyond 0.95, indicating the applicability of eqn (1) to make an association between relaxivities and the characteristic parameter Xr/Z of adsorbed cations. Most strikingly, the cumulants a_i are close to zero at $i = 1, 3$ in longitudinal case and at $i = 0, 2, 4$ in transverse case (Table 2). This intriguing finding reminds us of the parity of Hermite polynomials, that is, $H_i(-z) = (-1)^i H_i(z)$. Along this line, we boldly propose a general formula of cumulants a_i according to the harmonic oscillator theory in quantum mechanics:

$$a_i = \sqrt{\frac{\alpha i!}{\sqrt{\pi}2^i}} \quad (2)$$

Here, α denotes the coefficient of x in the expression of z. Based on eqn (2), the values of a_0, a_2, and a_4 are calculated to be about 0.75, 0.53 and 0.92, respectively, and the values of a_1 and a_3 are calculated to be 0.53 and 0.65, respectively. Obviously, these calculated values are in excellent consistency with the corresponding fitting values in Table 2, and further validating the applicability of harmonic oscillator theory in our system. In this scenario, the nearly null value of a_1 and a_3 in longitudinal case reveals that the even-parity states of harmonic oscillators are dominant. Likewise, the odd-parity states of harmonic oscillators determines the transverse relaxivities due to $a_0 \approx a_2 \approx a_4 \approx 0$.

Table 1 Electronegativity, radius and atomic number of the adsorbed cations

Parameters	Ca^{2+}	Fe^{3+}	Na^{+}	Mg^{2+}	Zn^{2+}	Ni^{2+}	Co^{2+}	Cd^{2+}
Atomic number	20	26	11	12	30	28	27	48
Electronegativity	11.30	15.38	9.44	17.13	10.38	9.60	9.10	9.79
Radius (Å)	0.99	0.64	0.95	0.65	0.74	0.72	0.74	0.97

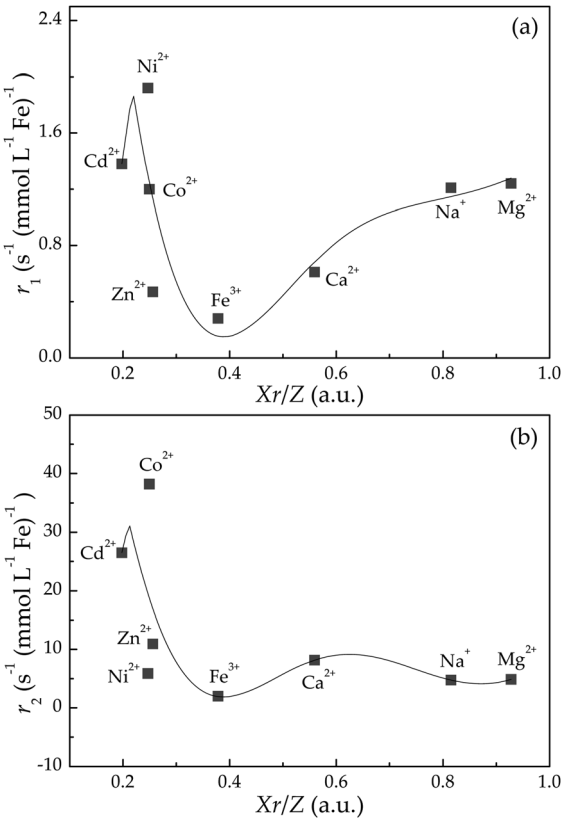

Fig. 3 Dependence of (a) r_1 and (b) r_2 values on Xr/Z with regard to various cation-adsorbed Fe_3O_4/γ-Fe_2O_3 nanoparticles. The experimental data are plotted as solid squares, and the solid lines are fitting results according to eqn (1).

In addition, the quantum mechanics gives the characteristic length (*i.e.*, $1/\alpha$) dividing classical forbidden area ($|z| > 1/\alpha$) and classical permissive area ($|z| \leq 1/\alpha$) for harmonic oscillators. In this work, z values can be calculated based on the fitting values of x_c and w according to the equation of $z = (Xr/Z - x_c)/w$. Fig. 4 shows that z values of Na^+ and Mg^{2+} cations are beyond $1/\alpha = 1$, indicating that the harmonic oscillations of Na^+ and Mg^{2+} cations around Fe_3O_4/γ-Fe_2O_3 nanoparticles are classical forbidden. By contrast, Ca^{2+}, Fe^{3+}, Zn^{2+}, Ni^{2+}, Co^{2+}, and Cd^{2+} cations can oscillate around Fe_3O_4/γ-Fe_2O_3 nanoparticles within classical permissive area.

Experimental

Synthesis and characterization

The pristine Fe_3O_4/γ-Fe_2O_3 nanoparticles were synthesized according to the method reported elsewhere[21,22] with little

Table 2 Fitting parameters according to eqn (1)

Relaxivity	r_{k0}	A	w	x_c	a_0	a_1	a_2	a_3	a_4
Longitudinal	3.95	-1.6×10^{-3}	0.37	0.26	0.73	4.5×10^{-5}	0.53	2.5×10^{-6}	0.89
Transverse	17.86	−19.33	0.38	0.29	1.2×10^{-3}	0.58	1.7×10^{-6}	0.66	8.9×10^{-8}

modification. Typically, 10 mL of Na_2CO_3 aqueous solution (0.6 mol L^{-1}) was added into 50 mL of $FeCl_3 \cdot 6H_2O$ aqueous solution (0.04 mol L^{-1}) and vigorously stirred for five minutes. After that, ascorbic acid (0.5 g) was added into the above solution and stirred for another ten minutes. Finally, the mixture was transferred into a Teflon-lined stainless-steel autoclave with a capacity of 100 mL for hydrothermal treatment at 160 °C for 3 h. After the autoclave had cooled down to room temperature naturally, the Fe_3O_4/γ-Fe_2O_3 precipitate was separated by centrifugation, washed successively with distilled water and absolute ethanol, and dried in the air at 60 °C for 4 h.

To mimic the actual element concentration in human body, the concentration of Ca^{2+}, Fe^{3+}, Na^+, Mg^{2+}, Zn^{2+}, Ni^{2+}, Co^{2+}, and Cd^{2+} cations was uniformly set to be 2 mmol L^{-1}. In a typical adsorption experiment, eight sets of 50 mg of the as-prepared Fe_3O_4/γ-Fe_2O_3 nanoparticles were separately soaked into 100 mL of $CaCl_2$, $FeCl_3$, NaCl, $MgCl_2$, $ZnCl_2$, $NiCl_2$, $CoCl_2$, and $CdCl_2$ aqueous solutions for 1 h. After the above adsorption, all precipitates were separated by centrifugation, washed successively with distilled water and absolute ethanol, and dried in the air at 60 °C for 4 h.

The X-ray diffraction (XRD) pattern of the sample was recorded with a Rigaku D/max-γB diffractometer equipped with a rotating anode and a Cu Kα source ($\lambda = 0.154056$ nm) at 40 kV and 150 mA between 10° and 80° (2θ) with a step size of 0.02°. The phase composition was further confirmed by X-ray photoelectron spectroscopy (XPS), which was performed on VG ESCALAB 220i-XL system. The morphology and structure of the sample was characterized by transmission-electron microscope (TEM) with an operating voltage of 200 kV (JEM-2100). The zeta potential values of the samples were determined by dynamic light scattering (DLS, Zetasizer Nano, Malvern Instrument). Iron concentrations in relaxivity experiments were determined by inductively coupled plasma-optic emission spectrometry (ICP-OES, PerkinElmer Optima 8000).

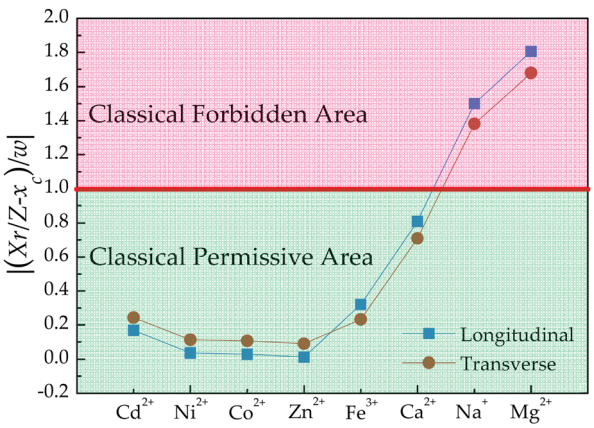

Fig. 4 Dependence of $(Xr/Z - x_c)/w$ values for various cation-adsorbed Fe_3O_4/γ-Fe_2O_3 nanoparticles.

Relaxivity measurement

A mq-60 NMR analyzer (Bruker Minispec) was applied to measure proton transverse (r_2) and longitudinal (r_1) relaxivities of the samples. Specifically, a certain amount of sample was dissolved in deionized water at 37 °C and laid in a magnetic field of 1.41 T with a frequency of 60 MHz. Then a Carr–Purcell–Meiboom–Gill spin-echo pulse sequence was adopted and the interecho time and repetition time were set to be 1 ms and 6 s, respectively. The as-measured signal data was fitted by a monoexponential decay curve to yield the T_2 relaxation time. On the other hand, an inversion recovery (IR) pulse sequence was adopted by using 10 inversion times between 0.05 and 10 s. Then a monoexponential recovery curve was utilized to fit the signal data to finally obtain T_1 relaxation time. All data were presented as arithmetic means of 3 replicates. After the measurements of T_1 and T_2, the relaxivities r_1 and r_2 could be obtained by fitting respective relaxation rate (s^{-1}) *versus* iron concentration (mmol L^{-1} Fe).

Conclusions

In summary, Ca^{2+}, Fe^{3+}, Na^+, Mg^{2+}, Zn^{2+}, Ni^{2+}, Co^{2+}, and Cd^{2+} cation-adsorbed Fe_3O_4/γ-Fe_2O_3 nanoparticles are synthesized by a facile soaking method to mimic actual element adsorption in human body. The r_1 and r_2 relaxivities of bare Fe_3O_4/γ-Fe_2O_3 nanoparticles are 3.86 and 17.41 s^{-1} $mmol^{-1}$ L, respectively. However, after cation adsorption, nearly all relaxivity values show a great decrease, manifesting surface-adsorbed cations greatly degenerate the MRI capability of iron-oxide contrast agents. Such relaxivity loss can be described by a modified GCAS function, taking into account of numerous harmonic oscillations of various cations around Fe_3O_4/γ-Fe_2O_3 nanoparticles. The quantum mechanics analyses show that even-parity and odd-parity states of harmonic oscillators are dominant in r_1 and r_2 relaxivities of cation-adsorbed Fe_3O_4/γ-Fe_2O_3 nanoparticles, respectively. Moreover, the harmonic oscillations of Na^+ and Mg^{2+} cations around Fe_3O_4/γ-Fe_2O_3 nanoparticles are found to be classical forbidden, which are quite different from their counterparts located in the classical permissive area.

Conflicts of interest

There are no conflicts to declare.

Acknowledgements

The authors are grateful to the financial aid from the National Natural Science Foundation of China (NSFC No. 51472133).

Notes and references

1 T. Shin, J. Choi, S. Yun, I. Kim, H. Song, Y. Kim, K. I. Park and J. Cheon, *ACS Nano*, 2014, **8**, 3393.
2 J. Y. Park, M. J. Baek, E. S. Choi, S. Woo, J. H. Kim, T. J. Kim, J. C. Jung, K. S. Chae, Y. Chang and G. H. Lee, *ACS Nano*, 2009, **3**, 3663.
3 Q. Wang, A. Xiao, Y. Liu, Q. Zou, Q. Zhou, H. Wang, X. Yang, C. Zheng, Y. Yang and Y. Zhu, *Nanomedicine*, 2018, **14**, 2551.
4 Y. Li, Y. Chang, R. Yuan and Y. Chai, *ACS Appl. Mater. Interfaces*, 2018, **10**, 25213.
5 I. Monaco, P. Armanetti, E. Locatelli, A. Flori, M. Maturi, S. Del Turco, L. Menichetti and M. C. Franchini, *J. Mater. Chem. B*, 2018, **6**, 2993.
6 Z. Zhao, C. Sun, J. Bao, L. Yang, R. Wei, J. Cheng, H. Lina and J. Gao, *J. Mater. Chem. B*, 2018, **6**, 401.
7 H. B. Na, I. C. Song and T. Hyeon, *Adv. Mater.*, 2009, **21**, 2133.
8 Q. A. Pankhurst, J. Connolly, S. K. Jones and J. Dobson, *J. Phys. D: Appl. Phys.*, 2003, **36**, R167.
9 H. U. Ahmed, A. Kirkham, M. Arya, R. Illing, A. Freeman, C. Allen and M. Emberton, *Nat. Rev. Clin. Oncol.*, 2009, **6**, 197.
10 J. W. M. Bulte and D. L. Kraitchman, *NMR Biomed.*, 2004, **17**, 484.
11 W. Liu, H. Dahnke, E. K. Jordan, T. Schaeffter and J. A. Frank, *NMR Biomed.*, 2008, **21**, 242.
12 C. A. Helms, *Am. J. Roentgenol.*, 1999, **173**, 234.
13 W. S. Seo, J. H. Lee, X. Sun, Y. Suzuki, D. Mann, Z. Liu, M. Terashima, P. C. Yang, M. V. McConnell and D. G. Nishimura, *Nat. Mater.*, 2006, **5**, 971.
14 C. Richard, B. T. Doan, J. C. Beloeil, M. Bessodes, E. Tóth and D. Scherman, *Nano Lett.*, 2008, **8**, 232.
15 J. Shin, R. M. Anisur, M. K. Ko, G. H. Im, J. H. Lee and I. S. Lee, *Angew. Chem., Int. Ed.*, 2009, **48**, 321.
16 J. S. Choi, J. H. Lee, T. H. Shin, H. T. Song, E. Y. Kim and J. Cheon, *J. Am. Chem. Soc.*, 2010, **132**, 11015.
17 Z. Li, J. F. Godsell, J. P. O'Byrne, N. Petkov, M. A. Morris, S. Roy and J. D. Holmes, *J. Am. Chem. Soc.*, 2010, **132**, 12540.
18 T. Yamashita and P. Hayes, *Appl. Surf. Sci.*, 2008, **254**, 2441.
19 T. Kim, E. Momin, J. Choi, K. Yuan, H. Zaidi, J. Kim, M. Park, N. Lee, M. T. McMahon, A. Quinones-Hinojosa, J. W. M. Bulte, T. Hyeon and A. A. Gilad, *J. Am. Chem. Soc.*, 2011, **133**, 2955.
20 W. A. Seo, J. H. Lee, X. Sun, Y. Suzuki, D. Mann, Z. Liu, M. Terashima, P. C. Yang, M. V. McConnell, D. G. Nishimura and H. Dai, *Nat. Mater.*, 2006, **5**, 971.
21 J. Ma, L. Cheng and K. Chen, *J. Appl. Phys.*, 2015, **117**, 154701.
22 J. Ma and K. Chen, *Sci. Rep.*, 2017, **7**, 42312.